Application of Asymmetric Surface Fabricated by Femtosecond Laser Process for Microparts Feeding

Atsushi Mitani[a] and Shinichi Hirai[b]

[a]Sapporo City University, 1 Geijyutsu-no-mori, Sapporo, Hokkaido 005-0864, Japan;
[b]Ritsumeiakn University, 1-1-1 Nojihigashi, Kusatsu, Shiga 525-8577, Japan

ABSTRACT

Femtosecond laser technology has the ability to form stable minute grating structures on various materials, including silicon wafers and stainless steel. By forming a periodic structure on a surface of sliding parts, the tribology characteristics can be improved, because the effect of adhesion decreases. Application of a double-pulsed femtosecond laser irradiation technique can generate periodic structures with asymmetric profiles. We previously showed that microparts, such as ceramic chip capacitors and resistors, can be fed along asymmetric surfaces using simple planar symmetric vibrations. Microparts move in one direction because they adhere to these surfaces asymmetrically. In this study, we tested the ability of an asymmetric surface microfabricated by the double-pulsed femtosecond laser irradiation technique to feed 0402-type capacitors (size, 0.4 x 0.2 x 0.2 mm; weight, 0.1 mg). Among the characteristics evaluated were the differences in profiles of the two inclined surfaces, the effect of decreased adhesion, the coefficient of friction in both the forward and the backward directions, and the friction angle of the 0402-type capacitors in both directions. Using the results of feeding experiments of these capacitors, we assessed the relationship between driving frequency and feeding velocity.

Keywords: Femtosecond laser process, Double-pulsed laser, Asymmetry, Microparts feeder

1. INTRODUCTION

Femtosecond laser technology is being utilized in various fields, including reshaping of materials, controlling chemical reactions, and microfabrication, as well as in micro-electro-mechanical systems (**MEMS**) technology, and the observation of super-high-speed phenomena. During microfabrication using femtosecond laser technology, materials situated around the irradiated area are chemically and thermally unaffected. This can lead to the formation of minute grating structures on various materials, including silicon wafers and stainless steel; these structures are of the same order of magnitude as the wavelength of the laser beam pulses. A periodic structure on a contacting surface can reduce the effects of friction and adhesion by decreasing the contact area.

We have previously shown that a saw-toothed surface with simple planar and symmetric vibrations can be used to feed microparts.[1] Because of differences in surface contact area between the sloping side of a tooth and the other side, microparts adhere more strongly in one direction than in the other. Adhesion is caused by electrostatic, van der Waal's, and intermolecular forces, as well as by surface tension, humidity, and inertia, all of which influence the motion of the microparts.[2] In addition, adhesion and friction are proportional to contact area. Thus, microparts will tend to move in one direction.

In the present study, we utilized femtosecond laser processing tools to design a microfabricated surface that can be used to feed **0402**-type capacitors (size, $0.4\times0.2\times0.2$mm; weight,0.1mm). The double-pulsed femtosecond laser irradiation technique was used to create an asymmetric microfabricated surface. Following inspection of the latter with an atomic force microscope (**AFM**) system, we designed a profile model of the microfabricated surface, and assessed its asymmetry. We also assessed the area of contact between the microfabricated surface and a **0402**-type capacitor.

Further author information: (Send correspondence to A. Mitani)
A. Mitani: E-mail: a.mitani@scu.ac.jp
S. Hirai: E-mail: hirai@se.ritsumei.ac.jp

Optomechatronic Technologies 2008, Otani, Bellouard, Wen, Hodko, Katagiri, Kassegne, Kofman, Kaneko, Perez, Coquin, Kaynak, Cho, Fukuda, Yi, Janabi-Sharifi, Eds., Proc. of SPIE Vol. 7266, 726614 • © 2008 SPIE • CCC code: 0277-786X/08/$18 • doi: 10.1117/12.807089

We also evaluated the tribology characteristics of the microfabricated surface relative to environmental parameters, especially ambient humidity. The coefficient of friction and the angle of friction of the **0402**-type capacitors were examined in both directions, as well as the differences in adhesion of the capacitors to fabricated and non-fabricated surfaces. Finally, we tested the ability of the microfabricated surface to feed **0402**-type capacitors, and we assessed the relationship between feeding velocity and vibration frequency, as well as the effect of feeding velocity on feeding stability.

2. RELATED WORKS

Many functional surfaces for microparts feeding have been developed using the Micro-Electro-Mechanical Systems (MEMS) technology. These include air flow actuators that realize micro motion and that can be used in conveyance systems.[3–9] Each actuator has driving and levitation nozzles. Air flows from the driving nozzles move microparts in the desired direction, while air flows from the levitation nozzles are used to raise the microparts from the surface, thus reducing adhesion and friction. In ciliary motion systems,[10–13] these actuators are composed of bimorph polyimide fabricated by the **MEMS** technology. Arrays of these actuators are moved in a wormlike manner to feed microparts in the desired direction. Micro fabricated actuator arrays present on a vibratory plate can generate vector force fields.[14–24] In this case, many actuator arrays are present on a vibratory plate. Each actuator is controlled by a computer program, which regulates contact between the vibratory plate and the micropart to accomplish the target manipulation.

We used the femtosecond laser processing tool to generate a functional surface with asymmetric tribologic and geometric characteristics but no actuators. Because microparts adhere more strongly in one direction than in the other, contact between the microparts and the functional surface varies according to the direction of motion.

Popular partsfeeders, including vibratory bowl-type[25–27] and linear feeders,[28–32] uses both the horizontal and vertical vibrations. In these systems, the aspect ratio of the horizontal and vertical vibration amplitudes must be adjusted to prevent parts from jumping. In our system, however, this adjustment is unnecessary because only horizontal vibration is used.

The objective of our research was to examine the dynamics of micrometer microparts. We found that the motion of these parts depends not only on inertia but on adhesion.

3. ANALYSIS OF MICRO-FABRICATED SURFACE

The feeder surface consists of a shim tape; i.e., a stainless material 0.5mm in thickness, 10mm in width, and 33mm in length. To generate a feeder surface with an asymmetrical profile, we used the double-pulsed femtosecond laser beam irradiation technique, in which a single axis femtosecond laser beam is divided in two by a splitter. One side of the beam has an angle of 20° and a delay of 50 ps. Transpiration of the surface of the material starts 50 ps after irradiation by the first beam. By irradiating with the second beam at the same time, transpiration recoil forces shift in the direction of the angle of incidence of the second beam, thus generating an asymmetric surface.

Fig. 1 shows a microphotograph of the microfabricated surface using the **AFM** system. Many periodic convexities were observed on the surface of the material. Analysis of the microphotograph yielded the surface profiles shown in **Fig. 2**. The period of the feeder surface was about $0.92\,\mu$m, the groove depth was $0.17\,\mu$m, and the roughness at the top of these convexities was about $0.025\,\mu$m. We examined the asymmetry of the feeder surface by evaluating inclinations of both sides of each convexity. As shown in **Fig. 3**, each convexity could be approximated by the polynomial:

$$y(x) = a_4x^4 + a_3x^3 + a_2x^2 + a_1x + a_0, \tag{1}$$

where x and y indicate the position and height in **Fig. 3**, respectively.

Each approximation function was transformed to its maximum value at the position $x = 0\,\mu$m. By averaging these approximation functions, we obtained the coefficient of each term shown in **Table 1**. To examine the asymmetry of these convexities, we calculated the inclination of the approximation function by solving its differential. The inclination was $y' = 0.42$ at the position $x = -0.25\,\mu$m and $y' = -2.2$ at the position $x = 0.25\,\mu$m, indicating that the inclination of the convexity was greater on the right side than on the left. That is, the two sides of the convexity were 32% asymmetrical.

Table 1. Coefficients of approximation functions(μm)

a_4	a_3	a_2	a_1	a_0
-2.97	- 4.75	-2.24	0	0

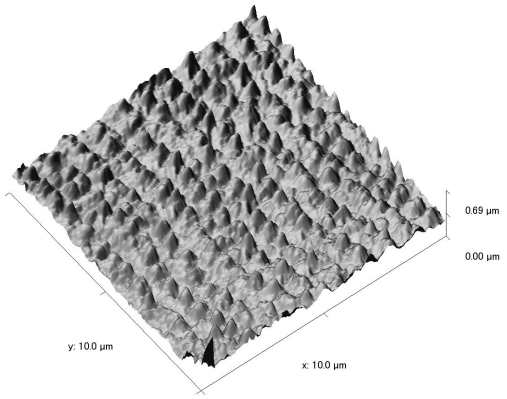

Figure 1. Micro-fabricated surface profile, as shown by the atomic force microscope (**AFM**)

4. EVALUATION OF FRICTION

4.1 Coefficients of Friction

To determine the tribologic characteristics of the microfabricated surfaces, such as friction and adhesion, we first measured its coefficient of friction using the **HEIDON TRIBOGEAR TYPE:HHS2000** (Shinto Scientific Co., Ltd.) friction tester. This friction tester has a globular point probe made of sapphire or diamond, which is in contact with a surface at a constant load. Friction is evaluated by measuring the resistance when the probe moves on the surface at a constant velocity. The experimental parameters are shown in **Table 2**. To determine the directionality of friction of the microfabricated surface, we compared movement from left to right (positive direction) and from right to left (negative direction). The resistance force over time in both directions is shown in **Fig. 4**. From these results, we obtained the dynamic coefficients of friction, which was 0.304 in the positive direction (μ_{pos}) and 0.329 in the negative direction (μ_{neg}), indicating that the asymmetry of friction on the microfabricated surface was about 7.6 %.

4.2 Angle of Friction of 0402-Type Capacitors

Next we measured the angle offriction of **0402**-type capacitors. To evaluate directionality, 35 capacitors were assessed three times each in the positive and negative directions. For comparison, similar experiments were performed using a non fabricated surface with only one direction because these surfaces have no directionality. Capacitors were placed on these surfaces, which were inclined until the capacitors fell, and we measured the angle of incline at which each capacitor started to fall. Some capacitors, however, remained on the surface even when the angle of incline exceeded 90°.

Table 2. Parameters of the friction tester **TRIBOGEAR**

probe	
material	sapphire
point radius	0.05 mm
test parameter	
load	100 g
velocity	10 mm/s

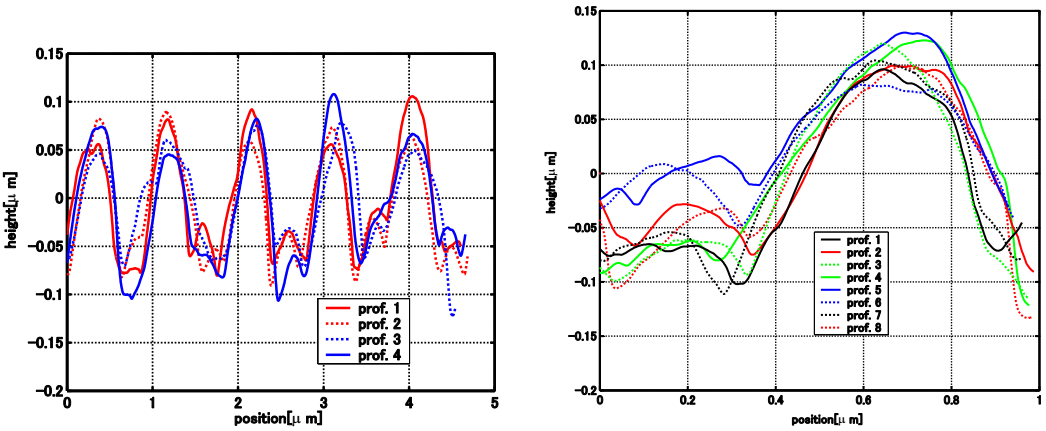

(a) Periodicity (b) Profiles of convexities

Figure 2. Analysis of the microfabricated surfaces

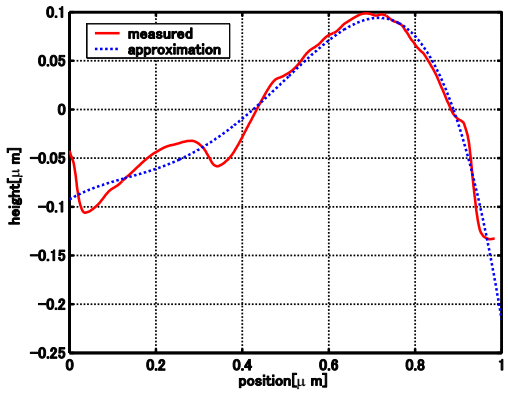

Figure 3. Approximation function of a convexity

Environmental factors, including ambient humidity and temperature, as well as van Der Waal' s and electrostatic forces, can affect adhesion, and therefore the movement of submillimeter-sized or smaller microparts. We therefore performed experiments at 50 %, 60 %, and 70 % ambient humidity and at a temperature of 24 ˚C. All experimental equipment and capacitors were equilibrated for one day in a sealed room at the desired humidity.

The experimental results are shown in **Fig. 5**. To estimate the effect of fabrication on adhesion, we compared the number of capacitors that fell. Despite the ambient humidity, this number was higher on microfabricated than on nonfabricated surfaces. For example, at 60% ambient humidity, 43 capacitors fell from the nonfabricated surface, whereas 65 and 61 capacitors fell from the microfabricated surface inclined in the positive and negative directions, respectively. These results indicate that microfabrication decreases adhesion, due to the decreased contact area between feeder surface and microparts.

We next assessed the effect of ambient humidity on adhesion. We found that 41, 43, and 25 capacitors fell at 50%, 60%, and 70% ambient humidity, respectively.When we assessed the differences between non fabricated and microfabricated surfaces, we found that the ratios at 50%, 60%, and 70% ambient humidity were 193%, 147%, and 154%, respectively. Therefore, both adhesion to the microfabricated surface and the decrease in adhesion caused by microfabrication were smallest at 60% ambient humidity.

When we evaluated the effect of ambient humidity on directionality of the angle of friction, we found that, at 50 %, 60 %, and 70 % humidity, the angle of friction in the positive direction was 1.6 %, 24%, and 14 % smaller, respectively, than the angle in the negative direction. Although there was directionality regardless of humidity, little was observed at 50 % humidity, whereas it was maximum at 60 % humidity.

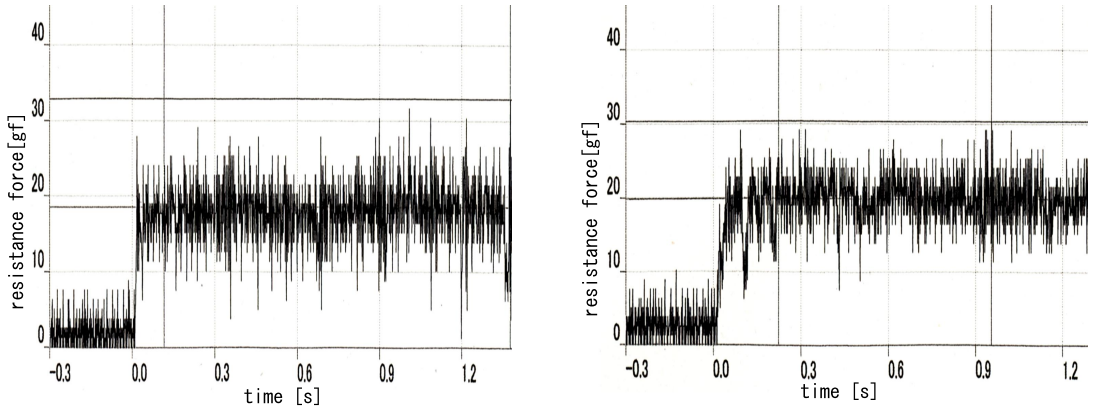

(a) positive direction (b) negative direction

Figure 4. Resistance over time observed when a probe moves on the surface at constant velocity

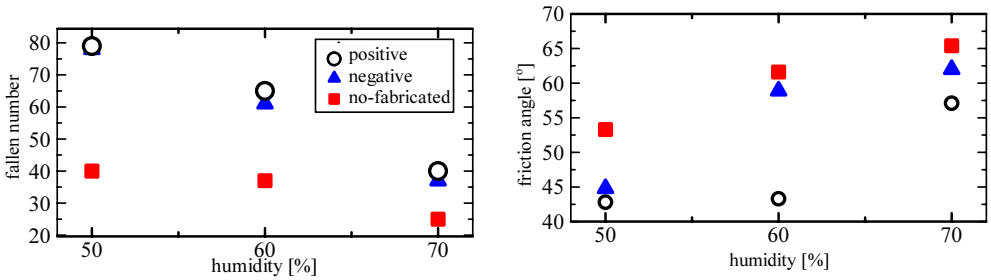

(a) Number of capacitors that fell from the microfabricated surface, of a total of 105 capacitors

(b) Average angle of friction of fallen capacitors. Capacitors that adhered were not considered

Figure 5. Experimental results of angle of friction of **0402**-type capactitors

5. ANALYSIS OF UNIDIRECTIONAL FEEDING

5.1 Surface Inspection of 0402-Type Capacitor

The surface profile of the **0402**-type capacitors was analyzed using a multi-purpose zoom microscope **MULTI-ZOOM AZ100** (Nikon Instruments Company) with a mono zoom optical system that enables on-axis observation and documentation and built-in optics of 1 × to 8 × magnification. When combined with an objective lens of up to 5 × magnification, we could take pictures at up to 40 × magnification. A digital camera was attached to the top of the microscope, and the pictures were forwarded to a computer via a USB interface. The resolution of forwarded pictures taken at 40× magnification was 0.276 μm/pixel.

Fig. 6(a) shows a microphotograph of a **0402**-type capacitor, which is composed of a conductor with an electrode on either side. Capacitor surface profiles were obtained using **Gwyddion** software, a modular program for **SPM** (scanning probe microscopy) data visualization and analysis (**Fig. 6**(b)). Because the electrodes protrude about 8 μm higher than surface of the conductor, these electrodes are in contact with the feeder surface. Since there are many convexities on the surface of these electrodes, we analyzed this contact by approximating a surface model of convexity using a second order polynomial:

$$f_p(x) = bx^2. \tag{2}$$

By averaging the approximation functions of some convexities, we defined the coefficient $b = -1.75e{-}02$ (**Fig. 7**). Finally, rotating the approximation function around the vertical axis yields a hyperbola model of the convexity on the surface of the capacitor electrode.

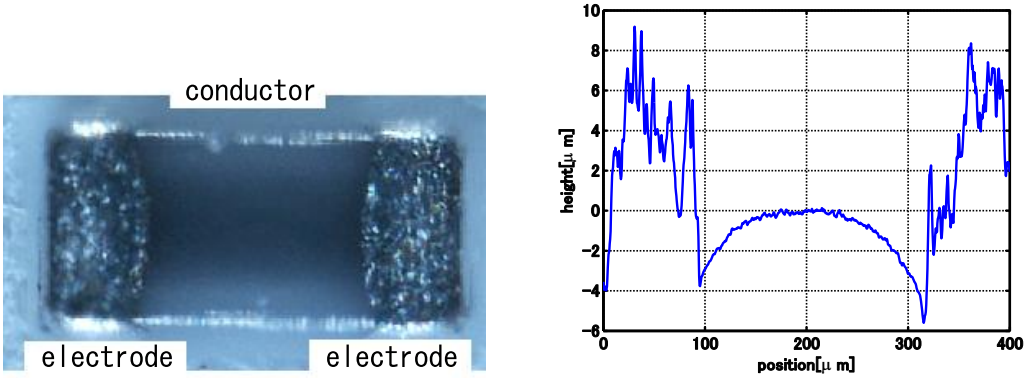

(a) Microphotograph (b) Surface profile

Figure 6. Details of an **0402**-type capacitor

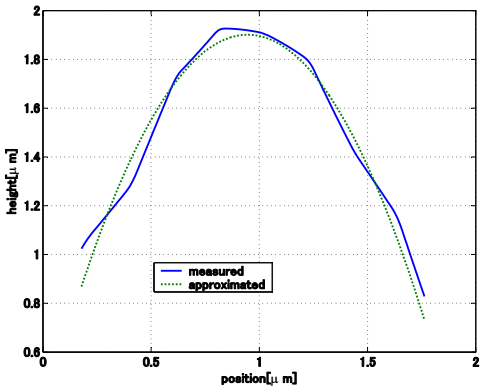

Figure 7. Convexity on the surface of an **0402**-type capacitor and its approximation

5.2 Analysis of Contact Between the Micro-Fabricated Surface and the Capacitor

When the two polynomials represented in equations **(1)** and **(2)** are in contact with each other, there is a shared tangent at the point of contact (**Fig. 8**). In this figure, we defined two coordinate systems: a parts coordinate system $O_p - x_p y_p$ and a surface coordinate system $O - xy$. The origins O_p and O were set at the extreme values of the approximation functions $y_p = f_p(x_p)$ and $y = f_s(x)$, respectively.

If ${}^oO_p(x_0, y_0)$ is the coordinates of the origin O_p of the surface coordinate system, equation **(2)** could be rewritten as a function at the surface coordinate system as:

$$y = b(x - x_0)^2 + y_0. \tag{3}$$

When two polynomials contact each other at $C(x_c, y_c)$, the shared tangent can be expressed as:

$$y = 2b(x_c - x_0)(x - x_c) + y_c. \tag{4}$$

If the angle of incline of the tangent is θ, the inclination of the tangent $y'(x)$ can be formulated as:

$$y'(x_c) = \tan\theta = 2b(x_c - x_0) = f_s'(x_c), \tag{5}$$

where

$$f_s'(x) \equiv \frac{\mathrm{d}f_s(x)}{\mathrm{d}x} = 4a_4x^3 + 3a_3x^2 + 2a_2x + a_1. \tag{6}$$

Then x_0 can be formulated as:

$$x_0 = x_c - \frac{f_s'(x_c)}{2b}. \tag{7}$$

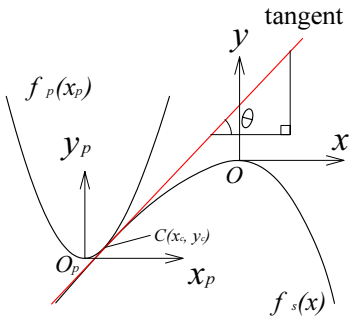

Figure 8. Surface models of the contact between a micropart and a microfabricated surface

By combining equations **(3)** and **(7)**, we obtain the equation:

$$y_0 = y_c - \frac{\{f_s'(x_c)\}^2}{4b}. \tag{8}$$

If adhesion occurs in the direction vertical to the tangent, we can formulate the distance between two polynomials. If a line perpendicular to the tangent intersects with the tangent at $Q(x_q, y_q)$ and intersects with the two polynomials at $Q_1(x_1, y_1)$ and $Q_2(x_2, y_2)$, respectively (**Fig. 9**), and if dl is the distance between these two polynomials, we obtain the equation:

$$dl = \overline{Q_1 Q_2} = \sqrt{(x_2 - x_1)^2 + (y_2 - y_1)^2}. \tag{9}$$

If the coordinate $Q_1(x_1, y_1)$ is already known, we can formulate the coordinate $Q_2(x_2, y_2)$. If the foot of the perpendicular from Q_1 to the tangent is known, the coordinate $Q(x_q, y_q)$ will correspond to the foot of the perpendicular from the coordinate Q_2. A function that passes through coordinates Q_1 and Q_2 can then be formulated as:

$$y = -\frac{1}{y'(x_c)}(x - x_1) + y_1. \tag{10}$$

If equation **(10)** is substituted into equation **(3)**, the coordinate $Q_2(x_2, y_2)$ can be obtained as:

$$x_2 = \begin{cases} x_0 - x_a & (y'(x_c) \neq 0), \\ x_1 & (y'(x_c) = 0), \end{cases} \tag{11}$$

$$y_2 = \begin{cases} y_0 + bx_a^2 & (y'(x_c) \neq 0), \\ b(x_1 - x_0)^2 + y_0 & (y'(x_c) = 0), \end{cases} \tag{12}$$

where

$$x_a \equiv \begin{cases} \dfrac{1}{2b}\left\{\dfrac{1}{y'(x_c)} - \sqrt{\dfrac{1}{y'(x_c)^2} - 4b\left(\dfrac{x_0 - x_1}{y'(x_c)} + (y_0 - y_1)\right)}\right\} & (y'(x_c) > 0), \\ \dfrac{1}{2b}\left\{\dfrac{1}{y'(x_c)} + \sqrt{\dfrac{1}{y'(x_c)^2} - 4b\left(\dfrac{x_0 - x_1}{y'(x_c)} + (y_0 - y_1)\right)}\right\} & (y'(x_c) < 0). \end{cases} \tag{13}$$

The distance becomes $dl = \infty$ because the equation **(3)** and **(10)** do not intersect when equation **(13)** has an imaginary root.

5.3 Contact Area that Causes Adhesion

Next we considered adhesion between the saw-toothed surface and a convexity on the surface of the capacitor. We defined the contact area as two surfaces mutually close enough to adhere to each other. If adhesion acts when the distance between two surfaces is smaller than δd, the colored area in **Fig. 10** can be defined as the contact area. In this figure, R_1 and R_2 are coordinates that become $dl = \delta d$. If the width of the feeder surface

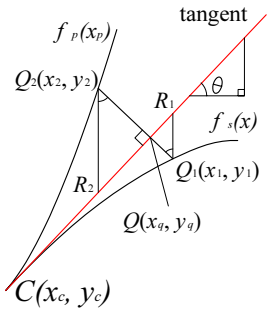

Figure 9. Distance between polynomials

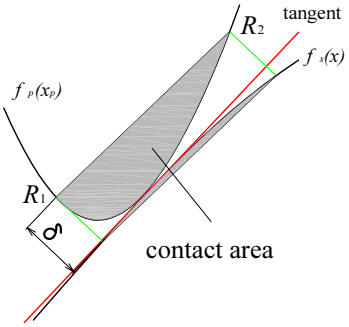

Figure 10. Adhesion model: adhesion acts between two surfaces within a distance δd

w is $-\infty \leq w \leq \infty$ in the depth direction perpendicular to the xy-plane, the contact area A can be defined as the sectional area cut out by a plane that passes through R_1 and R_2. Using the coordinates $R_1(x_{r1}, y_{r1})$ and $R_2(x_{r2}, y_{r2})$, the equation of the plane parallel to the z_p axis and passing through R_1 and R_2 can be formulated as:

$$y_p = c_r(x_p - x_{r1}) + x_{r1}^2, \tag{14}$$

where

$$c_r = \frac{y_{r2} - y_{r1}}{x_{r2} - x_{r1}}. \tag{15}$$

By formating the nodal line of the hyperbola and equation **(15)**, we obtained the equation:

$$(x_p - \frac{c_r}{2})^2 + z_p^2 = (x_{r1} - \frac{c_r}{2})^2. \tag{16}$$

Consequently, the contact area A can be described by the equation:

$$A = \pi(x_{r1} - \frac{c_r}{2})^2. \tag{17}$$

Fig 11 shows the simulated results of adhesion area relative to contact position and δ_d. We found that adhesion area is proportional to δ_d. The minimum contact area was observed at $x_c = 0.01\ \mu$m. We next compared the contact areas at $x_c \pm 0.2\ \mu$m. We calculated the ratio of contact area at both positions using the formula $r_A \equiv A(x_c = -0.2)/A(x_c = -0.2)$. We found that this ratio was $r = 3.2$ at $\delta d = 2.0$ and 2.4 at $\delta d = 1.0$. Thus, the microparts will adhere more strongly to the surface when they move from right to left. If $\delta d = 0.5$, the ratio became 1.0, indicating that adhesion directionality did not occur. When $\delta d = 0.1$, r was 0.3, indicating that, adhesion directionality was reversed. Consequently, adhesion directionality occurs when $\delta d > 0.5$.

6. FEEDING EXPERIMENTS OF 0402-TYPE CAPACITORS

6.1 Experimental Equipment

which is driven back and forth in a track by a pair of piezoelectric bimorph elements, powered by a function generator and an amplifier that delivers peak-to-peak output voltage of up to 300V.

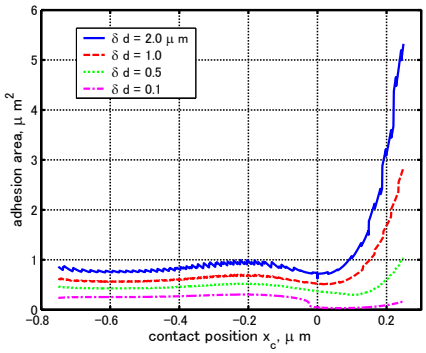

Figure 11. Relationship among contact position, δ_d, and adhesion area

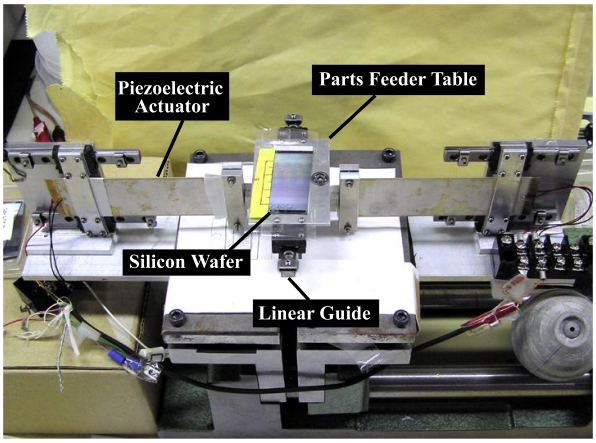

Figure 12. Micropart feeder using bimorph piezoelectric actuators

6.2 Feeding Experiments

Using a microfabricated shim tape, we performed feeding experiments of **0402**-type capacitors(**Video 1**). **Fig. 13** shows the relationship between driving frequency and feeding velocity of capacitors at driving frequencies $f = 120.5, 121.0, \cdots, 126.5$ Hz and vibration amplitude $A = 0.5$ mm. Experiments at each frequency were performed four times using 10 capacitors at ambient humidity of 70 % and a temperature of 25°C. The symbol ◯ represents each averaged velocity, and the symbol × represents measured velocity. Movement of the capacitors was recorded using a digital video camera at 30 fps. Velocity was calculated by counting the number of frames it took for a micropart to move 33 mm along the microfabricated surface. In addition, the variance of velocity (**Fig. 14**) was calculated according to equation **(18)**:

$$s^2 = \frac{1}{n-1} \sum_{i=1}^{n} (\bar{v} - v_i)^2, \tag{18}$$

where, n, $\bar{v}$, and v_i indicate the number of points, averaged velocity, and individual velocity, respectively.

6.3 Discussion

At frequencies $f \leq 122.0$ Hz, the average velocity was approximately 3.2 to 3.3 mm/s. The variance, however, tended to increase in proportion to the driving frequency. The maximum averaged velocity was 5.1 mm/s, realized at a frequency of $f = 124.0$ Hz, which could provide 765 parts par minute. The minimum variance was $s^2 = 0.50$ at a frequency $f = 125$ Hz, and the second smallest variance was $s^2 = 0.78$ at $f = 124.0$ Hz, which achieved maximum averaged velocity. As frequencies decreased to 123 Hz or less, the variance became larger as the driving frequency decreased. This finding indicates that the driving forces of the capacitors transferred from the feeder

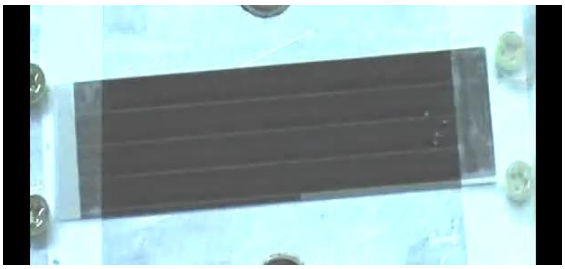

Video 1 Feeding experiments of **0402**-type capacitors http://dx.doi.org/10.1117/12.807089.1

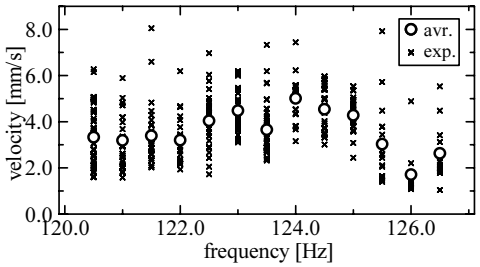

Figure 13. Relationship between frequency and velocity

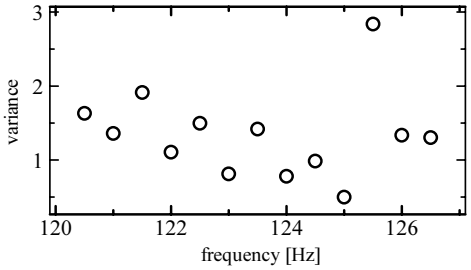

Figure 14. Variance of experimental results

surface were not sufficient to feed the capacitors steadily because the driving frequency decreases. In addition, the variance became largest at $f = 125.5\,\mathrm{Hz}$, and remained $s^2 \approx 1.4$ at $f = 126.0\,\mathrm{Hz}$ or larger. Consequently, the most stable feeding rate was achieved at frequencies of 124.0 to 125.0 Hz.

7. CONCLUSION

We have assessed the applicability of a microfabricated surface generated by femtosecond laser processing tools for microparts feeding. A double-pulsed femtosecond laser irradiation technique was used to microfabricate an asymmetric periodic profile surface on a stainless shim tape. The asymmetry of the microfabricated surface was evaluated by several methods. First, we derived surface profile models based on measurements using the **AFM** system. Next, coefficients of friction in both the positive and the negative directions were measured using a **HEIDON** friction testing tool. Finally, we performed experiments to measure the angle of friction of 0402-type capacitors in both directions. We also assessed the effects of ambient humidity on the angle of friction. We performed feeding experiments on **0402**-type capacitors using the microfabricated surface, and assessed the relationship between feeding velocity and driving frequency. We also determined the variance in measured velocities to determine steadiness of feeding.

In future studies, we will attemt to apply asymmetric surfaces generated by anisotropic etching process technology and the nanoimprint technology to the feeding of microparts.

ACKNOWLEDGMENTS

This research was supported in part by a Grant-in-Aid for Young Scientists (B) (No:20760150) from the Ministry of Education, Culture, Sports, Science and Technology, Japan, and by a grant from the Electro-Mechanic Technology Advancing Foundation(**EMTAF**), Japan.

REFERENCES

[1] Mitani, A., Sugano, N., and Hirai, S., "Micro-parts feeding by a saw-tooth surface", *IEEE/ASME Transactions on Mechatronics*, Vol.11, No.6, 671-681 (2006).

[2] Ando, Y. and Ino, J., "The effect of asperity array geometry on friction and pull-off force.", *Transactions of the ASME Journal of Tribology*, Vol. 119, 781-787(1997).

[3] Pister ,K.S.J., Fearing, R.S., and Howe, R.T., "A planar air levitated electrostatic actuator system", *Procs. of IEEE Micro Electro Mechanical System*, 67-71(1990).

[4] Fukuta, Y. et al., "Conveyor for pneumatic two-dimensional manipulation realized by arrayed MEMS and its control", *Journal of Robotics and Mechatronics*, Vol. 16, No. 2, 163-170(2004).

[5] Konishi, S. and Fujita, H., "A conveyance system using air flow based on the concept of distributed micro motion systems" *IEEE/ASME Journal of Microelectromechanical system*, Vol. 3, No. 2, 54-58(1994).

[6] Konishi, S. et al., "Experimental investigation of distributed conveyance system using air flow", *Procs. of 1998 International Symposium on Micro Mechatronics and Human Science*, 195-200(1998).

[7] Konishi, S., Mizoguchi, Y., and Ohno, K., "Development of a non-contact conveyance system composed of distributed nozzle units", *Procs. of 7th International Workshop on Emerging Technologies and Factory Automation* 593-598(1999).

[8] Arai, M. et al., "An air-flow actuator array realized by bulk micromachining technique", *Procs. of IEEJ the 19th Sensor Symposium*, 447-450(2002).

[9] Ku, P.-J. et al., "Distributed control system for an active surface device", *Procs. of the 2001 IEEE International Conference on Robotics and Automation*, 3417-3422(2001).

[10] Ataka, M. et al., "Fabrication and operation of polyimide bimorph actuators for a ciliary motion system", *IEEE/ASME Journal of Microelectromechanical System*, Vol. 2, No. 4,146-150(1993).

[11] Suh, J.W. et al., "CMOS integrated ciliary actuator array as a general-purpose micromanipulation tool for small objects", *Journal of Microelectromechanical Systems*, Vol. 8, No. 4, 483-496(1999).

[12] Suh, J.W. et al., "Fully programmable MEMS ciliary actuator arrays for micromanipulation tasks", *the Procs. of 2000 IEEE International Conference of Robotics and Automation*, Vol. 2, 1101-1108(2000).

[13] Ebefors, T. et al., "A robust micro conveyer realized by arrayed polyimide joint actuators", *Journal of Micromechanics and Microengineering*, Vol. 10, 337-349(2000).

[14] Oyobe, H., Kitajima, H., and Hori, Y., "Design and realization of autonomous decentralized object transfer system: magic carpet", *Procs. of 6th International Workshop on Advanced Motion Control*, 25-29(2000).

[15] Oyobe, H. and Hori, Y., "Object conveyance system "Magic Carpet" consisting of 64 linear actuators-object position feedback control with object position estimation", *Procs. of 2001 IEEE/ASME International Conference on Advanced Intelligent Mechatronics*, Vol. 2, 1307-1312(2001).

[16] Fukuda, T. et al., "Distributed control of flexible transfer system (FTS) using learning automata", *Procs. of the IEEE International Conference on Robotics and Automation*, 96-101(1999).

[17] Böhringer, K.-F., Donald, B. R., and MacDonald, N. C., "Upper and lower bounds for programmable vector fields with applications to MEMS and vibratory plate parts feeders", *International Workshop on Algorithmic Foundations of Robotics (WAFR)*, 255-276(1996).

[18] Böhringer, K.-F., Donald, B. R., and MacDonald, N. C., "Single-crystal silicon actuator arrays for micro manipulation tasks", *Procs. of the 1996 IEEE Workshop on Micro Electro Mechanical Systems (MEMS)*, 7-12(1996).

[19] Böhringer, K.-F., Donald, B. R., Mihailovich, R., and MacDonald, N. C., "Sensorless manipulation using massively parallel microfabricated actuator arrays", *Procs. of the 1994 IEEE International Conference on Robotics and Automation*, Vol. 1, 826-833(1994).

[20] Böhringer, K.-F., Donald, B. R., Mihailovich, R., and MacDonald, N. C., "A theory of manipulation and control for microfabricated actuator arrays", *Proc. of IEEE Workshop on Micro Electro Mechanical Systems (MEMS)*, 102-107(1994).

[21] Böhringer, K.-F., Donald, B. R., and MacDonald, N. C., "What programmable vector fields can (and cannot) do: Force field algorithms for MEMS and vibratory plate parts feeders", *Procs. of 1996 IEEE International Conference on Robotics and Automation*, Vol. 1, 822-829(1996).

[22] Böhringer, K.-F., Bhatt, V., and Goldberg, K., "Sensorless manipulation using transverse vibrations of a plate", *Procs. of 1995 IEEE International Conference on Robotics and Automation*, Vol. 24, 1989-1996(1995).

[23] Böhringer, K.-F., "Surface modification and modulation in microstructures: controlling protein adsorption, monolayer desorption and micro-self-assembly", *Journal of Micromechanics and microengineering*, Vol. 13, S1-S10(2003).

[24] Böhringer, K.-F., "Algorithms for sensorless manipulation using a vibrating surface", *Algorithmatica*, 389-429(2000).

[25] Maul, G.P. and Thomas, M.B., "A systems model and simulation of the vibratory bowl feeder", *Journal of Manufacturing System*, Vol. 16, No. 5, 309-314(1997).

[26] Okabe, S., and Yokoyama, Y., "Study on vibratory feeders: calculation of natural frequency of bowl-type vibratory feeders", *ASME Journal of Mechanical Design*, Vol. 103, 249-256(1981).

[27] Morrey, D. and Mottershead, J. E., "Modelling of vibratory bowl feeders", *Proceedings of the Institute of Mechanical Engineers, Part C, Mechanical Engineering Science*, Vol. 200, No. C6, 431-437(1986).

[28] Wolfsteiner, P. and Pfeiffer, F., "The parts transportation in a vibratory feeder", *IUTAM Symposium on Unilateral Multibody Contacts*, 309-318(1999).

[29] Frei, P. U., "An intelligent vibratory conveyer for the individual object transportation in two dimensions", *Procs. of the 2002 IEEE/RSJ International Conference on Intelligent Robots and Systems*, 1832-1837(2002).

[30] Morcos, W. A., "On the design of oscillating conveyors – case of simultaneous normal and longitudinal oscillations –", *ASME Journal of Engineering for Industry*, Vol. 92, No. 1, 53(1970).

[31] Barnes, R. N., "A novel design of a vibratory feeder incorporating an integral cut off valve", *Procs. of International Conference on Bulk Materials Handling and Transportation*, 315-319(1992).

[32] Carvalho, J. C. M. and Dahan, M., "Modelling a vibratory feeder: a new viewpoint", *Applied Simulation & Modelling*, 127-130(1990).